Title

INITIAL CHARACTERIZATION OF A BGO-PHOTODIODE DETECTOR FOR HIGH RESOLUTION POSITRON EMISSION TOMOGRAPHY

Author

Derenzo, S.E.

Publication Date

1983-11-01

LBL-16952

Lawrence Berkeley Laboratory
UNIVERSITY OF CALIFORNIA

Presented at the IEEE 1983 Nuclear Science Symposium, San Francisco, CA, October 19-21, 1983; and to be published in the IEEE Transactions on Nuclear Science, NS-31, 1984 (in press)

INITIAL CHARACTERIZATION OF A BGO-PHOTODIODE DETECTOR FOR HIGH RESOLUTION POSITRON EMISSION TOMOGRAPHY

S.E. Derenzo

November 1983

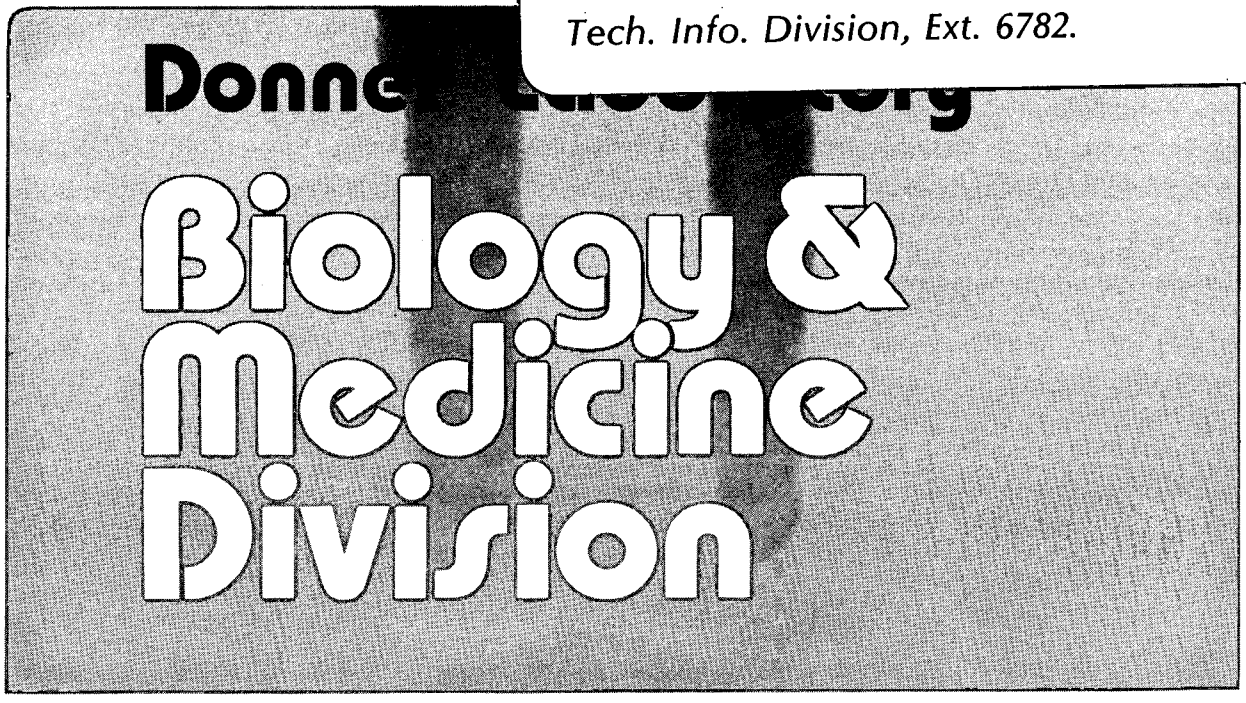

Prepared for the U.S. Department of Energy under Contract DE-AC03-76SF00098

LBL-16952

DISCLAIMER

LBL-16952

INITIAL CHARACTERIZATION OF A BGO-PHOTODIODE DETECTOR FOR HIGH RESOLUTION POSITRON EMISSION TOMOGRAPHY

Stephen E. Derenzo

Donner Laboratory
Lawrence Berkeley Laboratory
University of California
Berkeley, California 94720

November 1983

This work was supported by the U.S. Department of Energy under Contract No. DE-AC03-76SF00098 and N.I.H. Grnt P01 HL25840.

IEEE Trans Nucl Sci
NS-31, 1984 (in press)

INITIAL CHARACTERIZATION OF A BGO-PHOTODIODE DETECTOR FOR HIGH RESOLUTION POSITRON EMISSION TOMOGRAPHY*

Stephen E. Derenzo
Donner Laboratory and Lawrence Berkeley Laboratory
Berkeley, CA 94720

Abstract

Spatial resolution in positron emission tomography is currently limited by the resolution of the detectors. This work presents the initial characterization of a detector design using small bismuth germanate (BGO) crystals individually coupled to silicon photodiodes (SPDs) for crystal identification, and coupled in groups to phototubes (PMTs) for coincidence timing. A 3 mm x 3 mm x 3 mm BGO crystal coupled only to a SPD can achieve a 511 keV photopeak resolution of 8.7% FWHM at -150°C, using a pulse peaking time of 10 μs. When two 3 mm x 3 mm x 15 mm BGO crystals are coupled individually to SPDs and also coupled to a common 14 mm diam PMT, the SPDs detect the 511 keV photopeak with a resolution of 30% FWHM at -76°C. In coincidence with an opposing 3 mm wide BGO crystal, the SPDs are able to identify the crystal of interaction with good signal-to-noise ratio, and the detector pair resolution is 2 mm FWHM.

1. Introduction

In positron emission tomography of the brain, a spatial resolution of 2 mm FWHM is needed to measure the dynamics of blood flow in the cerebral arteries and the uptake and clearance of labeled tracers in small structures[1]. The primary difficulty in designing a positron tomograph with this spatial resolution lies not in the range of the positrons[2,3], nor the deviations from 180° emission[4], nor the detection properties of small BGO crystals[5], but in the size of available PMTs. Approaches to achieve a spatial resolution finer than the size of the PMTs include the use of lightpipes[6,7], partial coupling of PMTs to various faces of a close-packed array of smaller crystals[7,8], one dimensional light-proportion position logic[9-13], selective splitting of light among several PMTs so that the crystal producing the light may be identified[14,15], the use of pulse shape discrimination for different scintillator materials on the same PMT[16,17], and grid wires for localized gating of electrons from the photocathode to the first dynode[18-21].

This paper presents the initial characterization of a detector design using small bismuth germanate (BGO) crystals individually coupled to silicon photodiodes (SPDs) for crystal identification, and coupled in groups to phototubes (PMTs) for coincidence timing[3,22]. Our Monte Carlo computer code[23] calculated that the largest fraction of light is collected when the SPD and PMT are coupled to the full area of orthogonal faces of the crystal (Figure 1).

In addition, this paper describes the use of forward Compton scatters to enhance detection efficiency without sacrificing spatial resolution, and the advantages of position-sensitive SPDs to measure the depth-of-interaction in the crystal.

*Supported by D.O.E. Contract DE-AC03-76SF00098 and N.I.H. Grant P01 HL25840.

2. Properties of Silicon photodiodes

Table 1 lists our measurements of some of the properties of four commercial SPDs. At -100°C, and at reverse bias voltages below breakdown, dark current is below 1 pA for all diodes listed.

For an abrupt diode (i.e. having an abrupt change in donor/acceptor concentration between P-I-N layers), the depletion depth D (in μm) is given by[24]

$$D = 0.5 \sqrt{\rho V_e} \qquad (1)$$

where ρ is the resistivity of the silicon in ohm-cm, $V_e = V_i + V_b$ is the effective diode potential, V_i is the built-in potential and V_b is the external bias. The capacitance C (in pF) is given by

$$C = 106\ A/D \qquad (2)$$

where A is the area in mm^2. D is limited by the physical thickness of the silicon wafer.

We measured the capacitance of the four SPDs at a temperature of -100°C for approximately 25 voltages from zero to the breakdown voltage. Equations 1 and 2 did not describe these data, but an excellent fit was obtained in all cases when Equation 1 was replaced by the empirical expression

$$D = 0.5 \sqrt{\rho V_e / (1 + V_e/V_d)} \qquad (3)$$

where V_d is a voltage that corresponds to the asymptotic upper limit of D,

$$D \to D_a = 0.5 \sqrt{\rho V_d} \quad \text{as} \quad V_e \to \infty \qquad (4)$$

and

$$C \to C_a = 106\ A/D_a \quad \text{as} \quad V_e \to \infty \qquad (5)$$

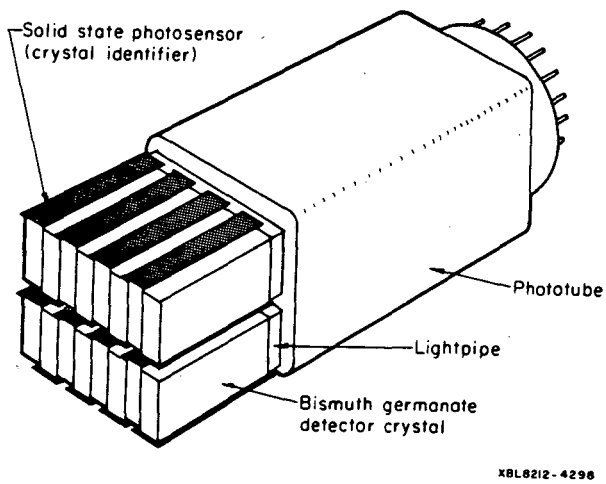

Figure 1: Schematic of multiple-crystal array where the energy deposited in each crystal is measured by individually coupled silicon photodiodes (SPDs) and the coincident time information is provided by a common phototube (PMT).

Table 1. Characteristics of four commercial silicon photodiodes

Manufacturer	Hamamatsu	Hamamatsu	Hamamatsu	Applied Solar Energy[a]
Model	S1722-01	S1722X	S1863X	H101
Sensitive area	4 mm diam (12.6 mm^2)	5 mm diam (19.6 mm^2)	10 mm x 10 mm (100 mm^2)	2.0 mm diam (3.1 mm^2)
Breakdown voltage	180 V	200 V	80 V	50 V
Capacitance near breakdown	11.8 pF	7.2 pF	35 pF	3.7 pF
Corresponding depletion depth	113 μm	289 μm	303 μm	89 μm
Capacitance at V_b= 0V	55 pF	133 pF	309 pF	23 pF
V_b= 1V	24 pF	81 pF	173 pF	15 pF
V_b= 2V	20 pF	48 pF	140 pF	9.1 pF
V_b= 5V	15 pF	29 pF	103 pF	6.0 pF
V_b= 10V	14 pF	21 pF	80 pF	4.7 pF
V_b= 20V	13 pF	16 pF	61 pF	4.1 pF
V_b= 50V	12 pF	11 pF	43 pF	3.7 pF
V_b=100V	12 pF	8.5 pF	-----	-----
V_b=200V	-----	7.2 pF	-----	-----
Results of fit by eqn (3):				
Resistivity ρ (ohm-cm)	14,000	4,300	7,700	4,400
Built-in reverse bias V_i	-0.18 V	-0.28 V	-0.76 V	-0.20 V
V_d	3.7 V	116 V	93 V	8.4 V
$V_e \to \infty$ capacitance C_a	11.8 pF	5.8 pF	25 pF	3.4 pF
$V_e \to \infty$ depletion depth D_a	113 μm	354 μm	423 μm	96 μm

[a]Applied Solar Energy Corporation, City of Industry, CA

The best fit parameters ρ, V_i, and V_d are given in Table 1. The S1722X and S1863X were fabricated from 500 μm silicon wafers and exhibit the lowest capacitance per unit area (0.35 pF/mm^2). However, the capacitance could be further reduced through the use of higher resistivity silicon and doping techniques that do not reduce the resistivity of the I-layer.

The semiconductor HgI_2 is also being developed as a scintillation photodetector[25,26], but is not yet commercially available.

3. Characteristics of the BGO-photodiode detector

3.1 Photopeak amplitudes and resolutions vs gamma ray energy

As described in Reference (27), a selected 3 mm x 3 mm x 3 mm BGO crystal (Harshaw Chemical Co., Solon, Ohio) was coupled to a Hamamatsu S1722-01 SPD and coated with a dry MgO reflector. Below -50°C, dark current is low and does not significantly contribute to amplifier noise. Using a 4393 FET, a SPD reverse bias of 10 V, a temperature of -150°C, and a pulse peaking time of 0.5 μs, the amplifier noise is 560 e$^-$ FWHM. The noise is reduced by longer peaking times, and is 300 e$^-$ FWHM at τ = 10 μs. The capacitive load of the charge amplifier (Figure 2) includes 15 pF from the FET and 12 pF from the SPD.

The best photopeak resolution was observed at a temperature of -150°C and a peaking time of 10 μs. Under these conditions, the photopeak amplitude and resolution were measured for several gamma ray energies (Table 2). A typical ^{22}Na spectrum (Figure 3) shows the 511 keV and 1275 keV photopeaks with FWHM = 8.7% and 5.4%, respectively.

3.2 Intrinsic luminosity and light collection from BGO

To determine the intrinsic luminosity of BGO, we used a 10 mm x 10 mm x 3 mm deep BGO crystal with one 10 mm x 10 mm face polished and the other 5 faces roughened and painted black. In such a crystal, only photons within a ±45° cone can escape total internal reflection in the BGO (n=2.15) and enter the PMT window (n=1.52).

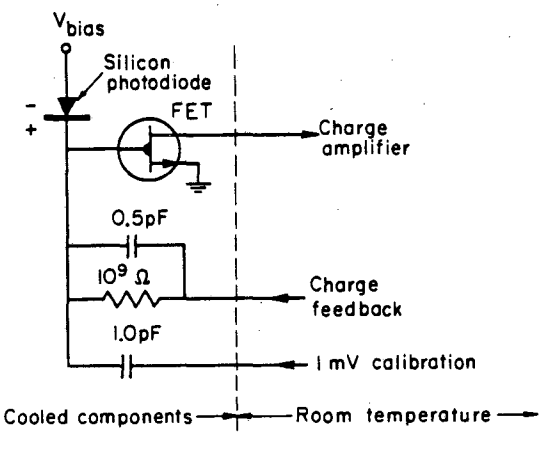

Figure 2: Circuit diagram of cooled components of charge amplifier. Subsequent pulse shaping consisted of equal RC integration and differentiation.

Table 2. Photopeak response of a 3 x 3 x 3 mm^3 BGO crystal and a S1722-01 SPD at -150°C, τ=10 μs, and 10V reverse bias

Source	E_γ (keV)	photopeak amplitude (e^-)	photopeak FWHM	amplitude per E_γ (e^-/keV)
^{133}Ba	80	870	46%	10.9
^{57}Co	122	1,290	38%	10.5
^{133}Ba	356	4,080	13%	11.5
^{22}Na	511	5,990	8.7%	11.7
^{137}Cs	662	7,800	7.2%	11.8
^{22}Na	1275	15,100	5.4%	11.8
^{60}Co	1332	15,800	5.3%	11.9

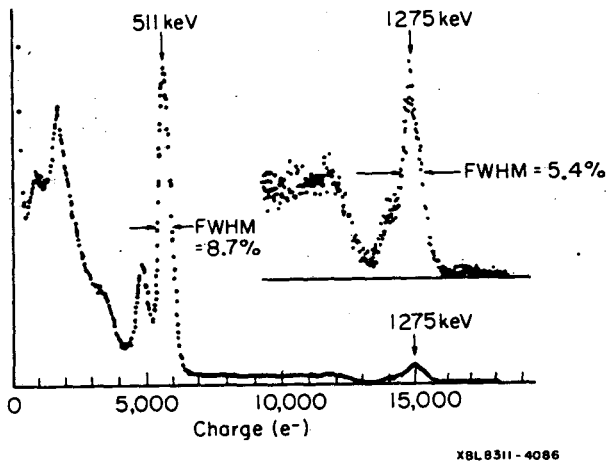

Figure 3: Pulse height spectrum from ^{22}Na taken with a 3 mm x 3 mm x 3 mm BGO crystal and a S1722-01 SPD, using a peaking time of 10 μs and at a temperature of -150°C.

Our Monte Carlo computer code calculated that 12.7% of the scintillation photons will exit the black BGO crystal, assuming a scattering length of 1 m, an absorption length of 1 m, and a diffuse reflectivity of 3%. Suppressing either the scattering or absorption changed the collection fraction by less than 0.2%. This insensitivity is due to the short paths (avg = 3.5 mm) that the photons travel in the crystal before they are either collected or absorbed. Changing the assumed reflectivity to 0% and 6% resulted in collection fractions of 12.0% and 13.3%, respectively.

At a temperature of -100°C, the black BGO crystal has a 662 keV photopeak amplitude of 2800 e^- using a Hamamatsu S1863X SPD. Assuming a quantum efficiency of 65%[28], we conclude that 2,800/(0.13 x 0.65) = 33,000 photons are produced in the BGO crystal, or 50 photons per keV. Since each photon has approximately 2.6 eV, this corresponds to an intrinsic energy efficiency of 50 x 2.6 eV per keV = 13%.

At a temperature of +20°C, a polished 3 mm x 3 mm x 3 mm deep BGO crystal coated with MgO reflector has a 662 keV photopeak amplitude of 3,200 e^- using a S1722 SPD. At -100°C the amplitude is 8,000 e^-, which is a 2.5-fold increase. At +20°C the intrinsic luminosity of BGO is thus 33,000/2.5 = 13,200 photons or 20 photons per keV (20 x 2.6 eV per keV = 5% energy efficiency).

We have used a PMT to measure the light output of a good-quality NaI(Tl) crystal relative to a black NaI(Tl) crystal, as well as the BGO crystals discussed above. The white NaI(Tl) crystal is 30 mm diam x 30 mm deep and has a 662 keV photopeak resolution of 8.5% FWHM. Its output is 2.5X larger than a 12 mm x 12 mm x 3 mm deep NaI(Tl) crystal painted black, which has a calculated collection fraction of 18%. The collection fraction for the white NaI(Tl) crystal is thus 18% x 2.5 = 45%. Its output is also 8 times larger than a BGO crystal having a similar collection fraction. Since the bialkali photocathode used has about 30% more quantum efficiency for NaI(Tl) (420 nm) than for BGO (480 nm), the luminosity ratio between the two materials is about 6. Thus the intrinsic luminosity of NaI(Tl) at 20°C is about 120 photons per keV and the intrinsic efficiency is about 120 x 3.0 eV per keV = 36%. The energy efficiency for light exiting the crystal is 36% x 45% = 16%, in reasonable agreement with the 13% measured by Van Sciver[29,30].

4. Crystal identification with silicon photodiodes

To demonstrate the use of SPDs to identify individual BGO crystals, we used the test set-up shown in Figure 4. The upper PMT was coupled to a single 3 mm x 10 mm x 30 mm deep BGO crystal. The lower PMT was coupled to two 15 mm x 3 mm x 3 mm wide BGO crystals. Each of the lower crystals was also coupled to an S1722-01 SPD. The separation between opposing detectors was about 25 cm, and a ^{22}Na line source was placed between them. A wire mesh at cathode potential was placed between the crystals and the front face of the lower PMT to prevent coupling of PMT pulses to the very sensitive charge amplifiers. If this precaution is not taken, the charge amplifiers detect artifact pulses whose amplitudes depend on the PMT voltage. The lower PMT, BGO crystals, SPDs, and associated charge amplifier components (Figure 2) were cooled to -76°C with an 8 liter, three-stage refrigeration unit (FTS Systems, Inc., Stone Ridge, NY).

Figure 5 shows the pulse height spectra from SPD B taken with a gated pulse height analyzer. The gate pulse was derived from a coincidence between the two phototubes using thresholds of 400 keV. When the ^{22}Na source is directly between the upper BGO crystal and crystal A (source position -1.5 mm), the pulse height spectrum seen on SPD B consists primarily of noise pulses (Figure 5a). When the source is directly between the upper crystal and crystal B (source position + 1.5 mm), the pulse height spectrum consists primarily of 511 keV photopeak pulses (Figure 5c). The photopeak resolution is 30% FWHM, poorer than the resolution given in Table 2, due to the higher temperature, light losses in the longer crystals, and the sharing of light with the PMT.

Figure 6 shows the coincident response of opposing 3 mm wide BGO crystals as the ^{22}Na source was moved in 0.25 mm steps along a line between them. The curve marked phototube is the coincident response of the two PMTs. Since the lower PMT cannot distinguish between the two BGO crystals, the response is relatively broad with a FWHM of 2.9 mm. The curve marked photodiode A is the coincident response of the two PMTs and SPD A, determined as the number of counts

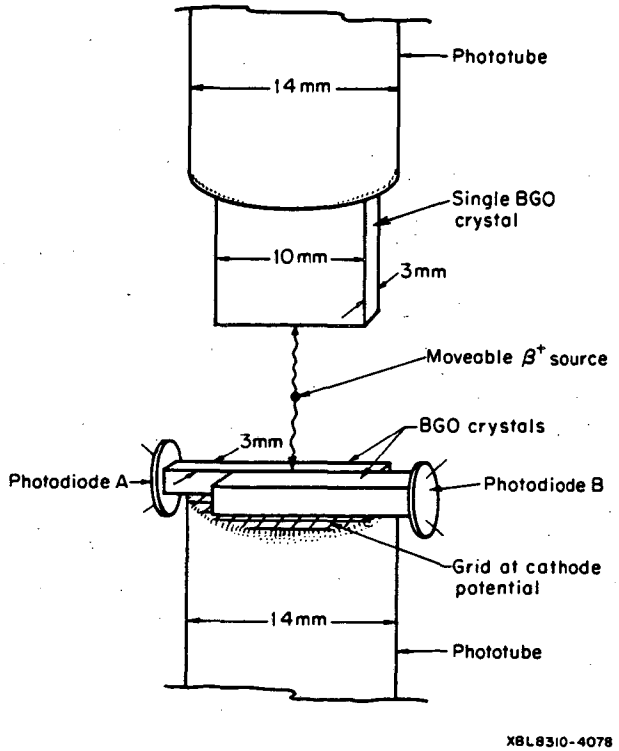

Figure 4: Sketch of experimental set-up where two crystals are coupled to a common PMT and coupled individually to SPDs.

above 310 keV in the SPD A pulse height spectrum as seen by the gated pulse height analyzer. The curve marked photodiode B is the coincident response of the two PMTs and SPD B. The curve marked photodiode A + B is the sum of the photodiode A and photodiode B curves and is equal to 90% of the phototube curve. The 10% difference is primarily due to Compton scattering in one of the lower crystals followed by photoelectric absorption in the other crystal.

5. Tomograph Design Factors

5.1 Advantages of position sensitive photodetectors

There are three primary advantages to the use of depth-of-interaction information: (1) Parallax error due to penetration in the crystals from off-axis sources can be essentially eliminated. (2) By rotating all crystals in the same direction (Figure 7), it is possible to use the penetration effect to achieve essentially continuous sampling without detector motion. (3) Time-of-flight tomographs suffer from a loss in timing resolution because the scintillation photons travel more slowly than the incident annihilation photons. As a result, the timing resolution is significantly poorer for long crystals than for shorter crystals, resulting in a trade-off between timing resolution and detection efficiency[31]. By knowing the depth of interaction, the timing resolution can be improved for long, efficient crystals.

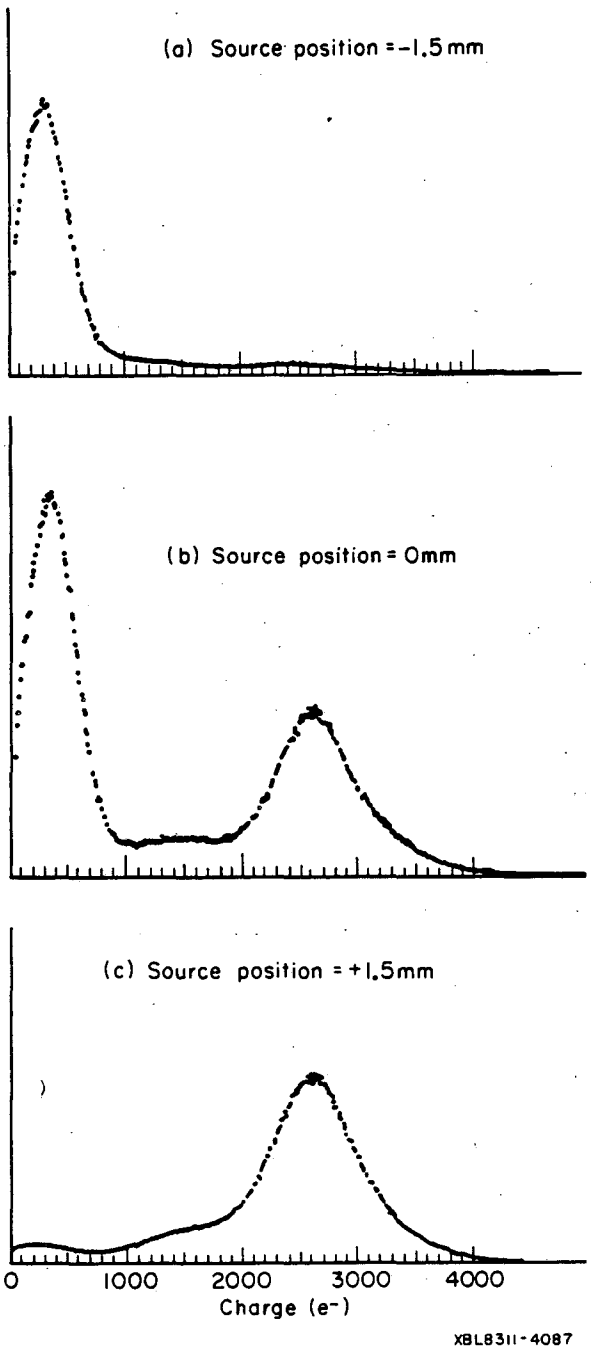

Figure 5: Pulse height spectra for photodiode B of Figure 4, gated by coincidences between two >400 keV PMT pulses. The 3 mm wide upper BGO crystal and the 1.2 mm diam ^{22}Na source define a narrow beam of annihilation photons.
(a) At a source position of -1.5 mm the beam intersects crystal A and the SPD B spectrum consists primarily of noise pulses.
(b) At a source position of 0 mm the beam intersects both crystals A and B.
(c) At a source position of +1.5 mm the beam intersects crystal B and the SPD B spectrum consists primarily of 511 keV photopeak pulses.

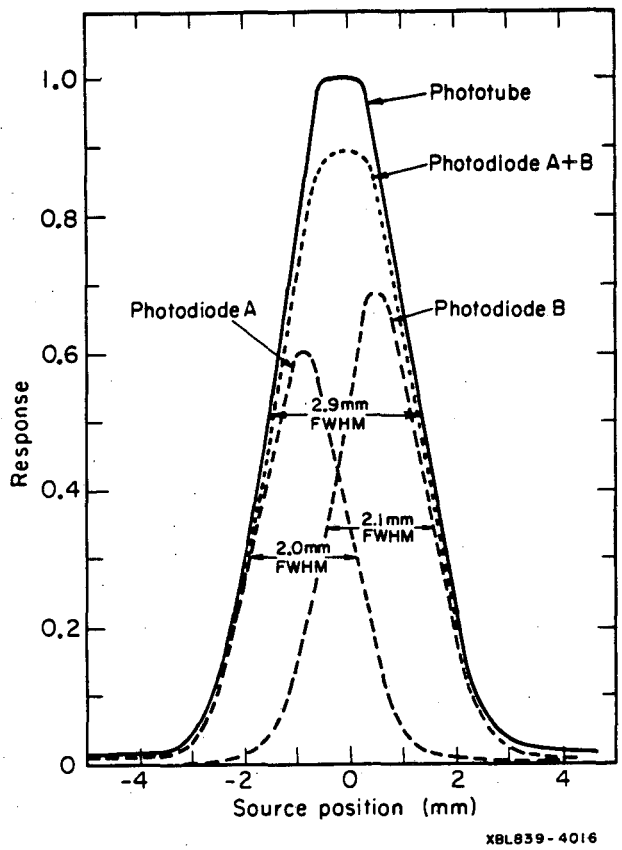

Figure 6: Coincident response function as a line source of ^{22}Na is moved between the opposing crystals shown in Figure 4. Phototube curve is response for two PMTs in coincidence. Photodiode A and Photodiode B curves are responses when the respective photodiode is in coincidence with both phototubes. Photodiode A+B curve is the sum of Photodiode A and Photodiode B curves.

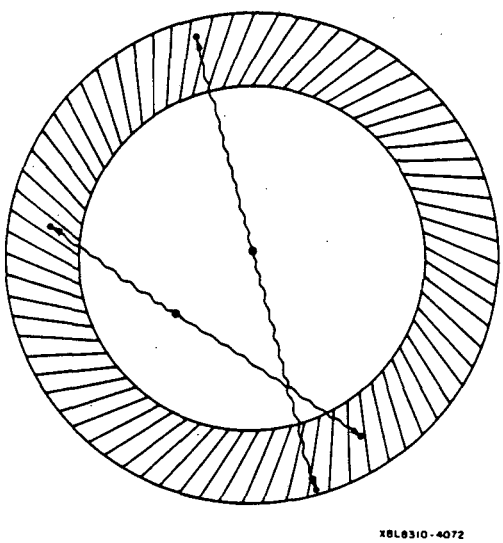

Figure 7: Scheme for rotating all crystals of a stationary positron detector ring so that depth-of-interaction information can be used to provide continuous linear sampling.

Fortunately, several manufacturers have developed the technology for producing position-sensitive SPDs. In these SPDs, leads are provided to each side of the P or N layer and the resistivity of that layer divides the signal according to the center of intensity of the incident light. Note that for BGO crystals of the shape shown in Figure 1, a two-segment SPD does not produce signals that are proportional to the position of interaction. Our calculations and experimental simulations using two PMTs indicate that the photons exiting the crystal have a spatially diffuse component and a sharper component corresponding to the $\pm 45^{o}$ total internal reflection escape cone. For interactions over most of the crystal, the escape cone falls only on one PMT and (except for a narrow region between the PMTs) the resulting signals are very insensitive to position.

5.2 Time-of-Flight positron tomography

BaF_2 is the material of choice for time-of-flight positron tomography[32], but the spatial resolution is presently limited by the size of high-quality PMTs necessary for sub-nanosecond timing. A fast PMT with a UV window could be coupled to groups of small BaF_2 crystals to detect the sub-nanosecond emission at 220 nm, and UV sensitive SPDs could be coupled individually to detect the slower 630 ns component at 300 nm.

5.3 Use of forward Compton scatters

Detector systems that reject multiple detector interactions do not suffer from a loss in resolution due to Compton scattering in the detectors. However, by increasing the complexity of the event trigger, it is possible to include forward Compton events and so increase the detection efficiency without degrading the spatial resolution.

Our Monte Carlo computer code was used to calculate the probability for one and two crystal photopeak events for a linear array of 3 mm x 10 mm x 30 mm deep BGO crystals (Table 3). Whenever two crystals are involved, and one has <170 keV energy deposition, it is almost always the crystal of first interaction. By including such events, the calculated photopeak efficiency is increased from 59% to 66% with little loss in spatial resolution.

6. Conclusions

Spatial resolution in positron emission tomography can approach 2 mm FWHM by using small BGO crystals individually coupled to cooled silicon photodiodes (SPDs) for crystal identification and coupled to a common phototube for coincident timing information. When a 3 mm x 3 mm x 3 mm BGO crystal is coupled only to a SPD at $-150^{o}C$, the 511 keV photopeak resolution is 8.7% FWHM. Two 3 mm x 3 mm x 15 mm BGO crystals coupled to a common PMT can be readily identified at $-76^{o}C$ by SPDs, even though the 511 keV photopeak resolution has been degraded to 30% FWHM by the higher temperature, light losses in the longer crystals, and the sharing of light with the PMT. The resulting detector pair resolution of 2 mm FWHM demonstrates the potential for a new class of ultra-high resolution positron emission tomographs.

Acknowledgements

We thank T. Vuletich, G. Chiao, and T. Ortiz for technical assistance, N. Servies and A. Kurahashi of Hamamatsu Corp. for providing silicon photodiodes, and T. Budinger, J. Cahoon, F. Goulding, D. Groom, E.

Table 3. Probability of 511 keV photopeak events involving 1 or 2 crystals in a linear array of 3 mm x 10 mm x 30 mm deep BGO crystals[a]

Event	Signature[b]	Probability	Localization[c]
Single crystal photopeak	E_1 = 511 keV	59.0%	Unique
Forward (<60°) scattering in crystal 1	E_1 < 170 keV E_2 = 511 - E_1	6.8%	Unique
Non-forward (60° to 180°) scattering in crystal 1	170 < E_1 < 340 E_2 = 511 - E_1	8.3%	Ambiguous
Multiple scattering in crystal 1, simulating forward scattering in crystal 2	340 < E_1 < 511 E_2 = 511 - E_1	0.7%	Erroneous

[a]10 mm x 30 mm crystal faces touching as shown in Figure 1, photons incident on 3 mm x 10 mm faces

[b]E_1 is the energy deposition in crystal of first interaction (crystal 1)
E_2 is the energy deposition in crystal of second interaction (crystal 2)

[c]Assuming photoelectric or single Compton-photoelectric events

Haller, R. Huesman, and D. Landis for helpful discussions. This work was supported in part by the Director, Office of Energy Research, Office of Health and Environmental Research of the U.S. Department of Energy, under Contract No. DE-AC03-76SF00098, and in part by the National Institutes of Health, National Heart, Lung, and Blood Institute under grant No. PO1 HL25840.

REFERENCES

1. Budinger TF, Derenzo SE, and Huesman RH: Instrumentation for positron emission tomography. Annals of Neurology, 1984 (in press)

2. Derenzo, SE: Precision measurement of annihilation point spread distributions for medically important positron emitters. In: Positron Annihilation, Hasiguti RR and Fujiwara K, eds, pp 819-823, The Japan Institute of Metals, Sendai, Japan, 1979

3. Derenzo SE, Budinger TF, Huesman RH, and Cahoon JL: Dynamic positron emission tomography in man using small bismuth germanate crystals. In Positron Annihilation, Coleman PG, Sharma SC, and Diana LM, eds. pp 935-945, North-Holland, New York, 1982

4. Colombino P, Fiscella B, Trossi L: Study of positronium in water and ice from 22 to -144 °C by annihilation quantum measurements. Nuovo Cimento 38: 707-723, 1965

5. Derenzo SE: Monte Carlo calculations of the detection efficiency of arrays of NaI(Tl), BGO, CsF, Ge, and plastic detectors for 511 keV photons. IEEE Trans Nucl Sci NS-28: No 1, 131-136, 1981

6. McIntyre JA: Plastic scintillation detectors for high resolution emission computed tomography. J Comput Assist Tomogr 4: 351-360, 1980

7. Derenzo SE, Budinger TF, and Vuletich T: High resolution positron emission tomography using narrow bismuth germanate crystals and individual photosensors. IEEE Trans Nucl Sci NS-30: No 1, 665-670, 1983

8. Ricci A, Hoffman E, Phelps M, et al: Investigation of a technique for providing a pseudo-continuous detector ring for positron tomography. IEEE Trans Nucl Sci NS-29: No 1, 452-456, 1982

9. Burnham C, Bradshaw J, Kaufman D, et al: One dimensional scintillation cameras for positron ECT ring detectors. IEEE Trans Nucl Sci NS-28: No 1, 109-113, 1981

10. Burnham C, Bradshaw J, Kaufman D, et al: Application of a one dimensional scintillation camera in a positron tomographic ring detector. IEEE Trans Nucl Sci NS-29: No 1, 461-464, 1982

11. Burnham C, Bradshaw J, Kaufman D, et al: A positron tomograph employing a one dimension BGO scintillation camera. IEEE Trans Nucl Sci NS-30: No 1, 661-664, 1983

12. Muehllehner G, Colsher JG, and Lewitt RM: A hexagonal bar positron camera: problems and solutions. IEEE Trans Nucl Sci NS-30: No 1, 652-660, 1983

13. Burnham CA, Bradshaw J, Kaufman D, et al: A stationary positron emission ring tomograph using BGO detector and analog readout. IEEE Trans Nucl Sci NS-31, 1984 (in press)

14. Murayama H, Nohara N, Tanaka E, et al: A quad BGO detector and its timing and positioning discrimination for positron computed tomography. Nucl Instr Meth 192: 501-511, 1982

15. Thompson CJ: Presented at the IEEE Nuclear Science Symposium, San Francisco, CA, October 19-21, 1983

16. Eriksson L: A high resolution positron camera. Proceedings of the VII Nobel Conference: "The Metabolism of the Human Brain Studied with Positron Emission Tomography", Karolinska Institute, Stockholm, May 17-20, 1983

17. Wong WH, Mullani NA, and Wardworth G: Characteristics of small barium fluoride (BaF_2) scintillator for high intrinsic resolution time-of-flight positron tomography. IEEE Trans Nucl Sci NS-31, 1984 (in press)

18. Charpak G: The localization of the position of light impact on the photocathode of a photomultiplier. Nucl Instr Meth 48: 151-153, 1967

19. Charpak G: Retardation effects due to the localized application of electric fields on the photocathode of a photomultiplier. Nucl Instr Meth 51: 125-128, 1967

20. Boutot JP and Pietri G: Photomultiplier control by a clamping cross-bar grid. IEEE Trans Nucl Sci NS-19: No 3, 101-106, 1972

21. Yamashita Y, Uchida H, Yamashia T and Hayashi T: Recent development in detectors for high spatial resolution positron CT. IEEE Trans Nucl Sci NS-31, 1984 (in press)

22. Barton JB, Hoffman EJ, Iwanczyk JS, et al: A high-resolution detection system for positron tomography. IEEE Trans Nucl Sci NS-30: No 1, 671-675, 1983

23. Derenzo SE and Riles J: Monte Carlo calculations of the optical coupling between bismuth germanate crystals and photomultiplier tubes. IEEE Trans Nucl Sci NS-29: No 1, 191-195, 1982

24. Moss TS, Burrell GJ, and Ellis B: Semiconductor Opto-electronics. John Wiley, New York, 1973, pp 184-185

25. Iwanczyk JS, Barton JB, Dabrowski AJ, et al: A novel radiation detector consisting of an HgI_2 photodetector coupled to a scintillator. IEEE Trans Nucl Sci NS-30: No 1, 363-367, 1983

26. Iwanczyk J, Dabrowski A, Markakis J, et al: Large area mercuric iodide photodetectors. IEEE Trans Nucl Sci NS-31, 1984 (in press)

27. Derenzo SE: Gamma-ray spectroscopy using small, cooled bismuth germanate scintillators and silicon photodiodes. Nucl Instr Meth, (in press), 1983

28. Technical data supplied by Hamamatsu TV Co., Ltd., Hamamatsu, Japan

29. Birks JB: The Theory and Practice of Scintillation Counting. Pergamon Press, Oxford, England, 1964, pp 473-474

30. W. Van Sciver, personal communication, 1983

31. Gariod R, Allemand R, Cormoreche E, et al: The "LETI" positron tomograph architecture and time of flight improvements. Proceedings of the Workshop on Time-of-Flight Tomography, pp 25-29. Washington University, St. Louis MO, May, 1982, (IEEE Cat. No. 82CH1791-3)

32. Laval M, Moszynski M, Allemand R, et al: Barium fluoride: inorganic scintillator for subnanosecond timing. Nucl Instr Meth 206: 169-176, 1983

Reference to a company or product name does not imply approval or recommendation of the product by the University of California or the U.S. Department of Energy to the exclusion of others that may be suitable.

This report was done with support from the Department of Energy. Any conclusions or opinions expressed in this report represent solely those of the author(s) and not necessarily those of The Regents of the University of California, the Lawrence Berkeley Laboratory or the Department of Energy.

Reference to a company or product name does not imply approval or recommendation of the product by the University of California or the U.S. Department of Energy to the exclusion of others that may be suitable.

TECHNICAL INFORMATION DEPARTMENT
LAWRENCE BERKELEY LABORATORY
UNIVERSITY OF CALIFORNIA
BERKELEY, CALIFORNIA 94720